Applied Physics Letters ARTICLE scitation.org/journal/apl

Chromaticity manipulation of indoor photovoltaic cells

Cite as: Appl. Phys. Lett. **118**, 043301 (2021); doi: 10.1063/5.0039653
Submitted: 5 December 2020 · Accepted: 7 January 2021 ·
Published Online: 25 January 2021

View Online Export Citation CrossMark

Zhi-Hao Chen,[1] Hang Yin,[1,a)] Johnny Ka Wai Ho,[2] Li-Yong Cui,[3,a)] Shu Kong So,[2] and Xiao-Tao Hao[1,4,a)]

AFFILIATIONS

[1]School of Physics, State Key Laboratory of Crystal Materials, Shandong University, Jinan, Shandong 250100, People's Republic of China
[2]Department of Physics and Institute of Advanced Materials, Hong Kong Baptist University, Kowloon Tong, Hong Kong, People's Republic of China
[3]School of Physics and Electronic Sciences, Changsha University of Science and Technology, Changsha 410004, China
[4]ARC Centre of Excellence in Exciton Science, School of Chemistry, The University of Melbourne, Parkville, Victoria 3010, Australia

[a)]**Authors to whom correspondence should be addressed:** hyin@sdu.edu.cn; cly@csust.edu.cn; and haoxt@sdu.edu.cn

ABSTRACT

Organic photovoltaic cells are appealing as indoor illumination harvesters to drive off-grid electronics in the Internet of things. However, a desirable output power usually requires expansive and dark active layers to absorb sufficient incident photons. The deployment of such large-scale dark objects is detrimental to the elaborately designed indoor lighting environment and affects human visual perceptions. Here, we propose a free-contact strategy to adjust the chromaticity of the transmitted indoor light by applying one-dimensional photonic crystals. Combining photonic crystals with various transmittances outside the photovoltaic cells, the spectral power distribution of the transmitted light can be precisely manipulated to realize a broad and consecutive color modulation covering the region from blue to orange. For certain photonic crystals, the chromaticity of propagated light can be recovered close to the light source. This work presents a solution to relieve light-disturbing in the application of organic photovoltaic cells under indoor illuminations.

Published under license by AIP Publishing. https://doi.org/10.1063/5.0039653

Organic photovoltaics (OPVs) have exploited their application scenario into the indoor environment due to the strong overlaps of absorbance with the emission spectra of indoor light sources.[1–5] State-of-the-art OPV cells have achieved high power conversion efficiencies (PCEs) under indoor illumination conditions with multiple strategies, including wide-bandgap non-fullerene,[6,7] all-polymer indoor OPV cells,[8] and interlayer optimization.[9] For OPV cells with certain bulk heterojunctions (BHJs), the optimal device performance is achieved accompanied by a well-defined transmission spectrum, which is altered from the incident spectrum of indoor light source.[10,11] For example, PM6, the typical wide-bandgap polymer used in high-efficiency OPV cells, has intensive absorbance between 500 and 700 nm. This can severely influence both the indoor light illumination and visual perception.[6,12–14] Unlike the photovoltaic absorbers under the standard 1-sun illumination, light harvesters for indoor applications mainly absorb photons in the visible wavelength range. Thus, they are highly correlated with the daily activities of humans. Placing such large-scale and dark objects in the indoor environment would be detrimental to the visual perceptions for the following reasons. (i) Variation in the transmission spectrum inevitably leads to a change in chromaticity and illuminance. The deployment of such OPV cells would make the elaborate efforts on light manipulation at certain environments, e.g., hospitals, classrooms, shopping malls, and homes, in vain. (ii) To get high external quantum efficiency, the spectral photo response of OPV cells should match the indoor light sources, which is sensitive to the human visual perception, leading to a dilemma between efficiency and visual perception. Therefore, it is a critical issue of how much initial properties of interior lights can be retained after the introduction of light-absorbing cells. Nevertheless, improving the performance of indoor photovoltaic cells has received intensive research, whereas the interference in light source properties has barely received concerns and investigations so far.

To realize the preservation and manipulation of the indoor light chromaticity after OPV cells, photonic crystals (PCs) are potential candidates with a promising light-adjusting property. PCs are artificial materials or structures with periodic spatial variation of dielectric permittivity on the subwavelength scale.[15,16] The primary characteristic of photonic crystal is the photonic bandgap, which originates from

Published under license by AIP Publishing

multiple Bragg scattering. Photons located within the bandgap are prohibited from propagating.[17,18] Due to the ability to model the flow of light, PCs have captured attention for many potential applications, including omnidirectional mirrors,[19] Fabry–Pérot cavities,[20,21] optical filters,[22,23] and serving as a surface interface layer for light-emitting diodes with high brightness and solar cells with high conversion efficiencies.[24,25]

In this work, we demonstrate that one-dimensional (1D) PCs can effectively manipulate the transmitted light after indoor OPV cells to realize a free-contact wide-range chromaticity adjustment and a recovery of the incident light chromaticity. Herein, the 1D PC composed of SiO_2 and TiO_2 is rationally designed and fabricated based on transfer matrix simulation. Three selected BHJ blends are applied to verify the applicability of PCs. The result shows that the indoor light spectra can be adjusted by transmitting through the PC with varied component thickness to realize a color manipulation from blue (0.1695, 0.1760) to orange (0.5457, 0.4171). For certain PC structures, the transmitted light chromaticity can be effectively recovered to the original light color. The PC systems we designed exhibit capacity in recovering the color of interior light and preserving both the original applicability and visual perception.

In order to determine the most suitable PC structure for chromaticity manipulation of indoor light, we calculate the transmittance of a 1D PC $(AB)^N$ with different period N and various component thicknesses using the transfer matrix method. The components (A and B) are chosen to be SiO_2 and TiO_2 with a refractive index about 1.431 and 2.123, respectively.[26] In consideration of reasonably transmitted light intensity, the period is set to $N = 5$. The designed PC structure is illustrated by the schematic in Fig. 1(a), where the component layers of SiO_2 and TiO_2 are distinguished with different colors, and the electric field amplitudes of incident light (E_0), reflected light (rE_0), and transmitted light (tE_0) are marked in accompany with the transmission directions. Using the Maxwell equations to solve the electric and magnetic fields of two adjacent interfaces, the transfer matrix of a single layer can be obtained, which can be extended to solve the transmission and reflection coefficients of the 1D PC,

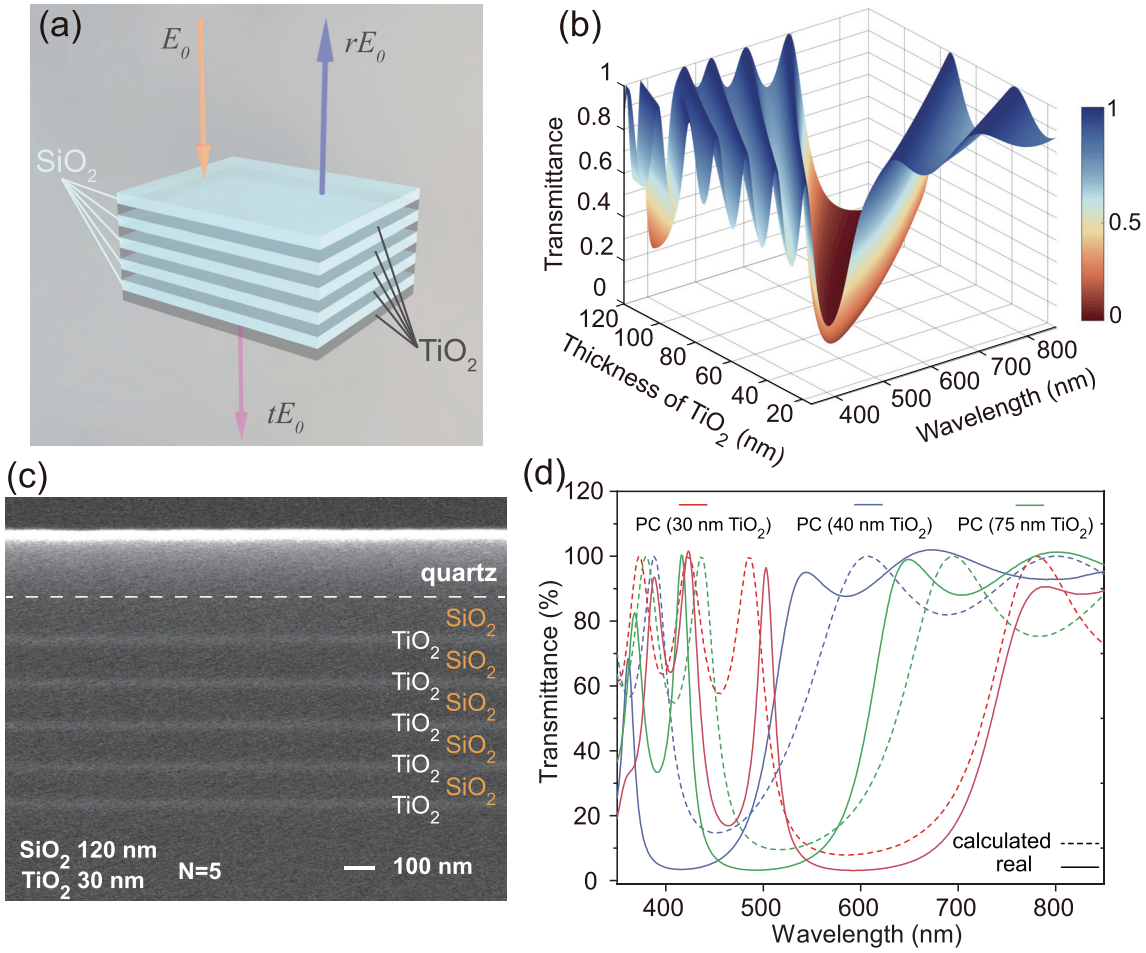

FIG. 1. (a) Schematic of the designed 1D PC structure composed of SiO2 and TiO2. (b) The calculated transmittance property of PC with 120 nm fixed SiO2 layers and 15 nm–120 nm varied TiO2 layers at an interval of 1 nm, period of 5. (c) TEM image of the fabricated 1D PC. (d) The comparation of the transmittance between calculated results and the measured data of the fabricated PCs.

Published under license by AIP Publishing

$$\begin{bmatrix} 1 \\ r \end{bmatrix} = \begin{bmatrix} M_{11} M_{12} \\ M_{21} M_{22} \end{bmatrix}^N \begin{bmatrix} t \\ 0 \end{bmatrix}, \tag{1}$$

where 1, t, and r represents the incidence, transmittance, and reflection coefficients, respectively. The 2×2 matrix is the transfer matrix of a unit cell of the PC, and M_{11}, M_{12}, M_{21}, and M_{22} are obtained according to the boundary conditions of the electric and magnetic fields. At normal incidence, they are given by

$$\begin{aligned} M_{11} &= e^{ik_1 d_A}\left[\cos k_2 d_B + \frac{1}{2} i\left(\frac{n_B}{n_A} + \frac{n_A}{n_B}\right) \sin k_2 d_B\right], \\ M_{12} &= e^{-ik_1 d_A}\left[\frac{1}{2} i\left(\frac{n_B}{n_A} - \frac{n_A}{n_B}\right) \sin k_2 d_B\right], \\ M_{21} &= e^{ik_1 d_A}\left[-\frac{1}{2} i\left(\frac{n_B}{n_A} - \frac{n_A}{n_B}\right) \sin k_2 d_B\right], \\ M_{22} &= e^{-ik_1 d_A}\left[\cos k_2 d_B - \frac{1}{2} i\left(\frac{n_B}{n_A} + \frac{n_A}{n_B}\right) \sin k_2 d_B\right], \end{aligned} \tag{2}$$

where k_1 (k_2) denotes the wave vector in layer A (B), and n_A (n_B) and d_A (d_B) denotes the refractive index and thickness of layer A (B), respectively. The transmittance is the ratio of the transmitted light intensity and incident light intensity, and the light intensity is proportional to the square of the electric fields. Then, the transmittance is given by

$$\begin{aligned} T &= |t|^2, \\ R &= |r|^2. \end{aligned} \tag{3}$$

We simulate four designed PC structures, and the results indicate that a structure of 120 nm fixed SiO_2 layers and 15–120 nm varied TiO_2 layer with a period of 5 [Fig. 1(b)] is the most promising candidate (the other three are shown in Fig. S1). It can be noticed that the transmittances of PCs exhibit a wide photonic bandgap accompanied by several periodic emerging peaks among the visible wavelength region. As the unit thickness increased, the wide-bandgap exhibits a redshift inclination. To manipulate the indoor light, the PC should have an adjustable photonic bandgap across the entire visible wavelength region while possessing reasonable transmittance, which is exactly achieved by the PC in Fig. 1(b). We further fabricate three kinds of 1D PCs in this structure with TiO_2 thicknesses of 30 nm, 40 nm, and 75 nm, respectively (the details of fabrication are summarized in the Supporting Information). Figure 1(c) shows the transmission electron microscope (TEM) image of PC with 30 nm TiO_2, in which the SiO_2 and TiO_2 layers in five periods can be clearly distinguished. The calculated and actual PC transmittance spectra are compared in Fig. 1(d). It shows that the sample spectra are matched well with the calculated results, indicating the accuracy of PC fabrication.

In the design of high-performance IPV cells, one of the most crucial principles is choosing donor and acceptor molecules of which the absorption spectra overlap well with the indoor light sources to harvest sufficient incident photons. Here, typical wide-bandgap polymer donors and wide-bandgap non-fullerene acceptors are selected to fabricate BHJ films, including PBDB-T:BTA3, PM6: O-IDTBR, and PTB7-Th: ITIC. The chemical structures and energy levels are

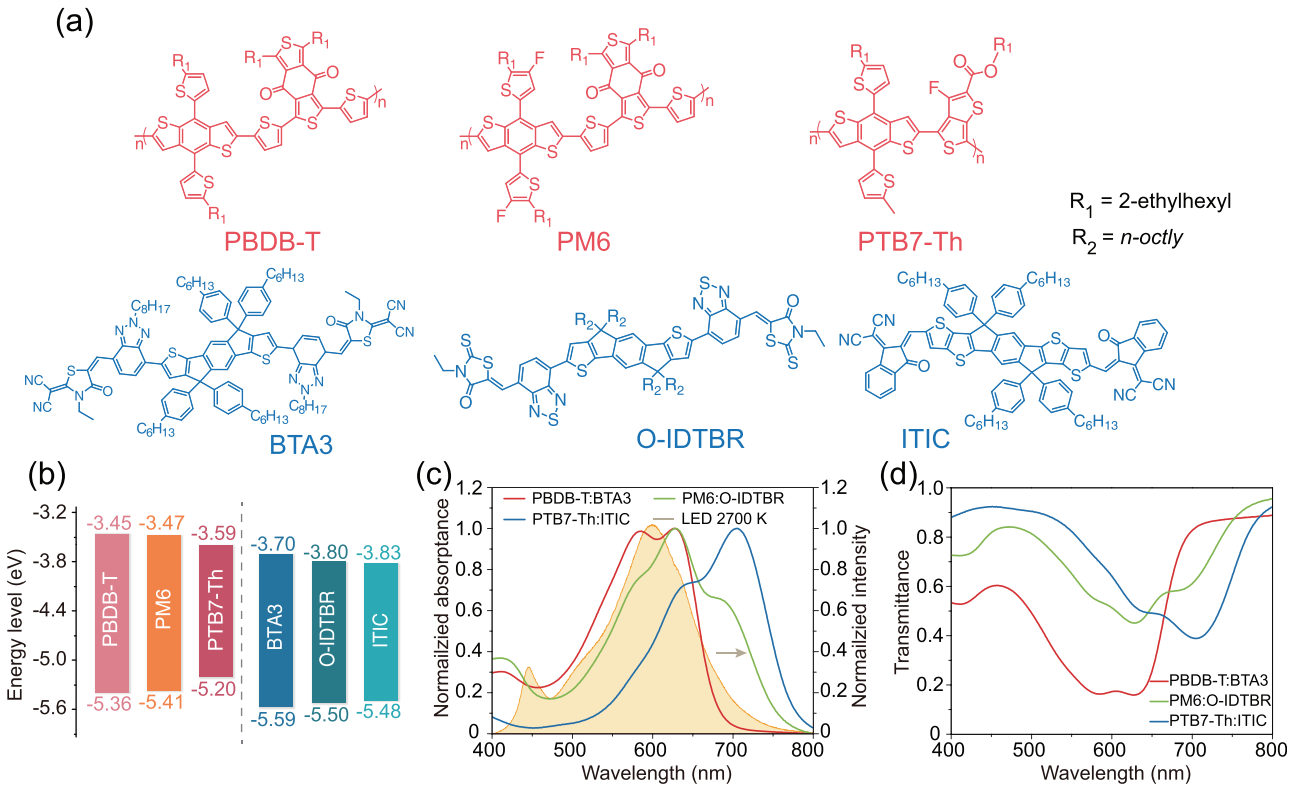

FIG. 2. (a) Chemical structures of the donors and acceptors used to compose BHJ films. (b) Energy level diagram of donor and acceptor molecules. (c) The absorption spectra and (d) the calculated transmittance spectra of PBDBT: BTA3, PM6:O-IDTBR, and PTB7-Th:ITIC. The yellow shade denotes the emission spectrum of 2700 K LED light source.

Published under license by AIP Publishing

summarized in Figs. 2(a) and 2(b), respectively. Figure S2 summarizes the absorbance and transmittance spectra of neat donors and acceptor films. The absorption spectra are all located in the visible region between 400 and 800 nm. A 2700K light-emitting diode (LED) is applied as the light source with an emission spectrum in a wavelength region from 400 to 700 nm. The absorption spectra of all BHJs partly or totally overlap with the emission spectrum of the LED, indicating their qualifications for indoor light harvest [Fig. 2(c)]. Based on the Beer–Lambert law, the transmittance of BHJ films can be calculated by the following equation:

$$T = 10^{-A}, \tag{4}$$

where A represents the film absorbance.[27] Figure 2(d) plots the calculated transmittance spectra of the four BHJ films. The transmittance intensities and spectral peak positions vary in different BHJ films. This diversity would result in interfered light propagated and influence the original light applications.

We fabricate OPV cells with the structure of ITO/ZnO/PBDB-T:BTA3/MoO_3/Ag, in which the Ag electrode is controlled in 100 nm and 30 nm to realize transparent cells (the experimental details are illustrated in the supplementary material). The J–V characteristics under AM 1.5 G and 1000 lux LED light are shown in Figs. 3(a) and 3(b), respectively, and the device parameters are summarized in Table I. For the conventional device with a 100 nm Ag layer, it achieves a short-circuit current density (J_{sc}) of 13.52 mA cm^{-2}, an open-circuit voltage (V_{oc}) of 1.10 V, a fill factor (FF) of 52.7%, and a power conversion efficiency (PCE) of 7.8% under AM 1.5 G, and a J_{sc} of 111.6 μA cm^{-2}, a V_{oc} of 0.99 V, an FF of 70.1%, and a PCE of 23.9% under a 1000 lux LED light. The low light intensity of LED illumination results in the significantly dropped J_{sc} value and leads to an extra V_{oc} loss since the trap-assisted recombination dominates under the scenario of low carrier density.[2,28,29] From outdoor to indoor, the decreasing light intensity will limit the bimolecular recombination, which promotes the FF.[30,31] When the anode thickness reduces to 30 nm, the device PCE drops to 5.5% and 11.5% under sun radiation and LED light, respectively. A severe decrease in J_{sc} can be observed, which originates from the dissipated energy loss of the transmitted photons. A thinner Ag electrode also introduces interfacial defects,

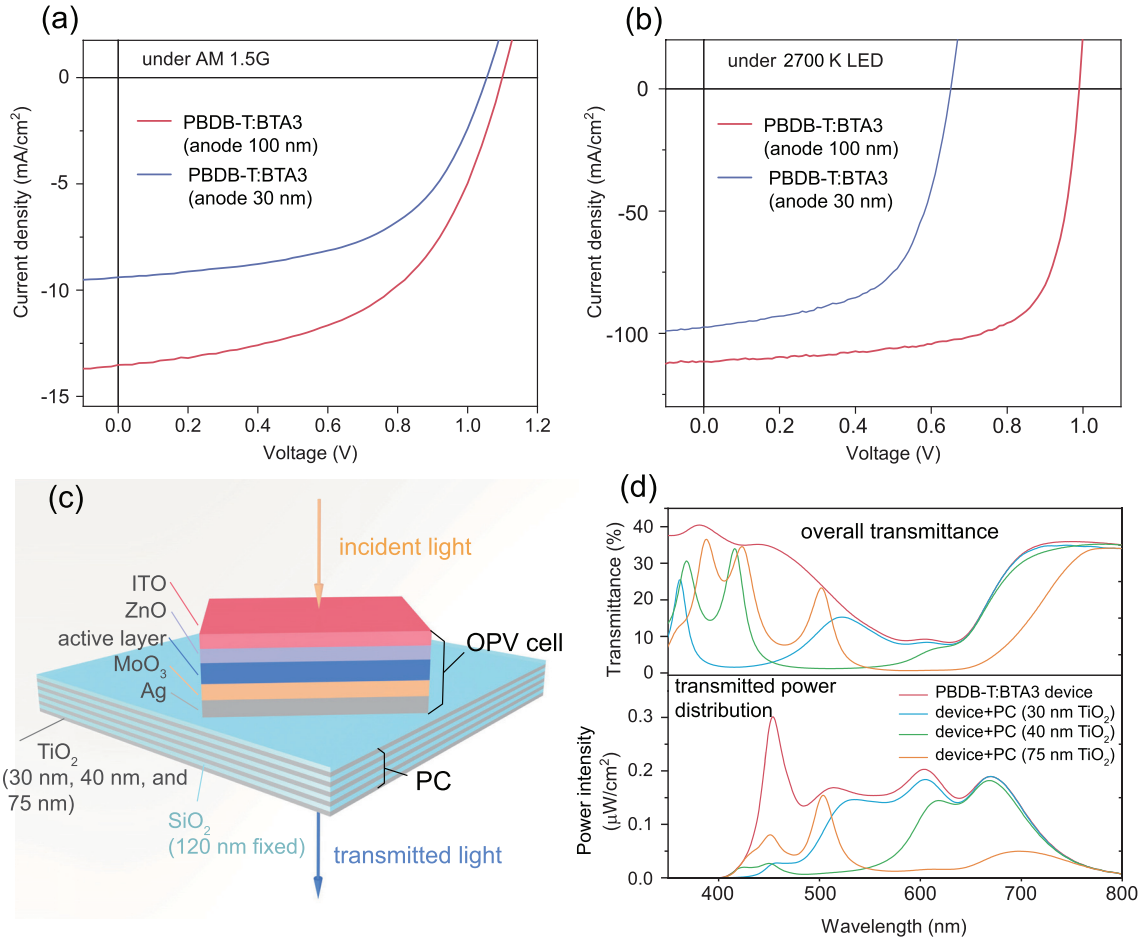

FIG. 3. (a) and (b), J–V characteristics of the conventional and transparent PBDB-T:BTA3-based OPV cells under 1-sun and 2700 K LED light at 1000 lux. (c) Schematic of the application of PC combined with the OPV cell to manipulate the transmitted light. (d) The transmittance spectra (top) and the transmitted power intensity spectra (bottom) of 2700 K LED after transparent OPV devices and devices combined with PCs.

Published under license by AIP Publishing

TABLE I. Photovoltaic parameters of the OPV cells under AM 1.5 G and 1000 lux 2700 K LED light.

Thickness of the anode	Light	P_{in} (mW cm^{-2})	J_{sc} (mA cm^{-2})	V_{oc} (V)	Fill factor (%)	P_{out} (mW cm^{-2})	PCE (%)
30 nm	AM 1.5 G	100	9.40	1.05	55.0	5.5	5.5
	1000 lux LED	0.324	0.0974	0.65	59.1	0.037	11.5
100 nm	AM 1.5 G	100	13.52	1.10	52.7	7.8	7.8
	1000 lux LED	0.324	0.1116	0.99	70.1	0.077	23.9

leading to extra trap-assisted recombination. It shows a minor influence on V_{oc} and FF under solar illumination but significantly affects the parameters under indoor light, a V_{oc} of 0.65 V and an FF of 59.1% as shown in Table I, which can be ascribed to the increased percentage of trap-assisted recombination in the device.

We combine all three kinds of the fabricated 1D PCs with the OPV device to investigate the transmittance property, where PCs are placed after the Ag electrode, as illustrated by the schematic in Fig. 3(c). The overall transmittance spectra and the transmitted power intensity distributions of the LED light at 1000 lux are shown in Fig. 3(d). After transmitting through OPV devices, the initial light power is overall weakened accompanied by the variation in spectral peak features. For instance, after propagation through the PBDB-T:BTA3 device, the light power reduces to around 0.2 μW cm^{-2} nm^{-1} among 450–600 nm. When further propagating through with PC layers, the transmitted power spectra exhibit obvious variations. For PC with 30 nm TiO_2, photons located below 550 nm can propagate through, while those located beyond 550 nm can hardly transmit. When the thickness of TiO_2 increases to 75 nm, only photons located between 600 and 750 nm can effectively pass through. The same manipulation can be realized in the other two BHJ-based OPV cells, as shown in Fig. S3.

To verify the color manipulation of 1D PCs on the light transmitted through BHJ films, we investigate the chromaticity and calculate CIE 1931 *xy* chromaticity coordinates. Figure 4(a) shows the PBDB-T:BTA3-based device and PC effects on the color of transmitted light. The chromaticity coordinates of the LED light source (0.4196, 0.4059) correspond to the reddish-yellow. After transmitting through the OPV device, the chromaticity is changed to near the pure white with a coordinate of 0.3128, 0.3373.

After the employment of the fabricated PCs after OPV cells, the transmitted light color can be effectively adjusted to orange (0.4214, 0.4181), red (0.5296, 0.3431), and cyan (0.1816, 0.3431), as exhibited in the demonstrations in Figs. 4(b)–4(e). We also calculate the chromaticity coordinates based on the simulated PC transmittance and plot in Fig. 4(a) with the thickness of TiO_2 layers varying from 15 nm

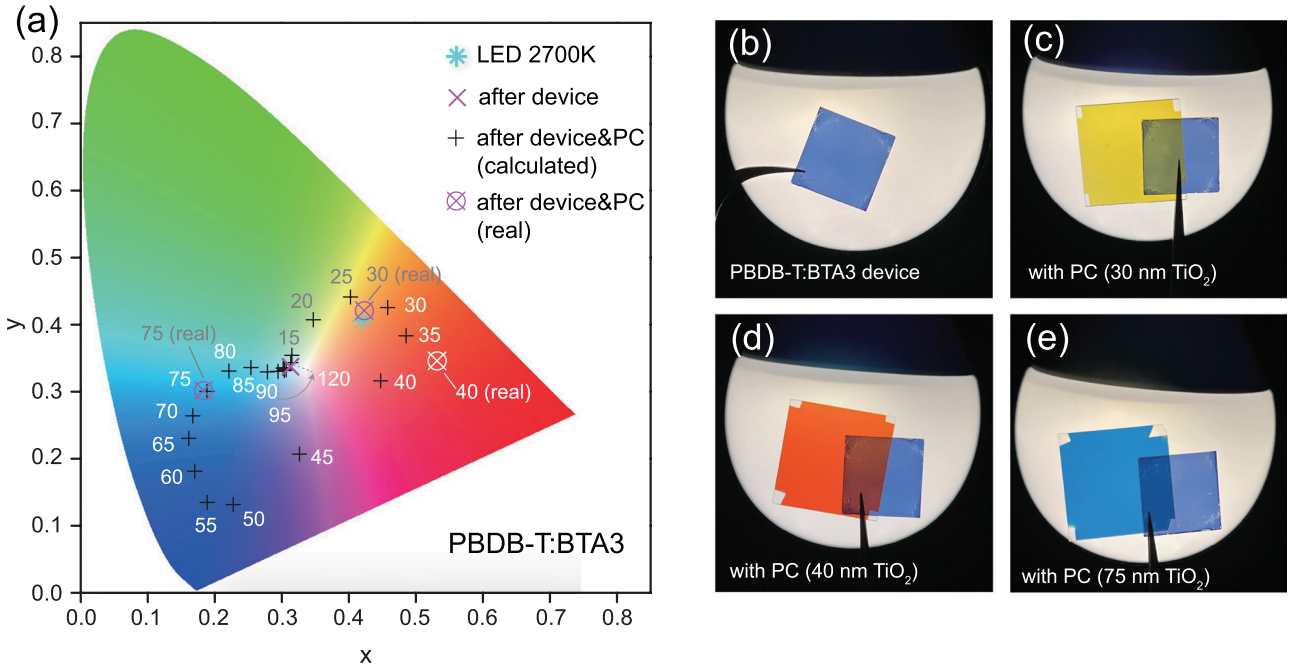

FIG. 4. (a) The CIE 1931 *xy* chromaticity diagram presenting the color coordinates of 2700 K LED light source, light transmitted through PBDB-T:BTA3-based device, and transmitted light through devices and PCs with both calculated and actual measured results. (b)–(e) Demonstration images of PBDB-T:BTA3-based device combined with PCs with different structures under 2700 K LED light.

Published under license by AIP Publishing

to 120 nm at an interval of 5 nm. It shows that the designed 1D PC can effectively manipulate the transmitted indoor light in a wide optical range. The measured and simulated results are matched with each other. The effectiveness of 1D PC in chromaticity manipulation also shows its validity in the BHJ systems of PM6:O-IDTBR and PTB7-Th:ITIC, as shown in Fig. S4. Furthermore, PCs with certain thicknesses can recover the transmission color close to the original light source. For example, the combination of PBDB-T:BTA3-based device and PC with 30 nm TiO_2 can achieve a transmission with a color coordinate of 0.4214, 0.4181, which is extremely close to the coordinate of 2700 K LED light.

In conclusion, we demonstrate the effectiveness of 1D PCs in manipulating the power distribution spectra of indoor light sources transmitted after OPV cells. Consecutive chromaticity manipulation can be effectively realized to convert a wide range of color features. For BHJ films that severely affect the chromaticity of incident lights, PCs with suitable component thicknesses are capable of recovering the original illumination. By deploying 1D PCs outside the OPV cell structure, the chromaticity of the interior light source can be easily adjusted for various applications in multiple scenarios, and the human visual perception can be effectively preserved or tuned. Meanwhile, the performance of transparent indoor OPV cells is discussed, showing that interfacial defect-induced trap-assisted recombination has a significant impact on the harvest of indoor photon energy. Specifically designed transparent electrodes might preserve a better device performance and replace the thin Ag electrode in future applications. The strategy proposed by this work resolves the dilemma between high device performance and unaffected light properties in the harvest of indoor light energy.

See the supplementary material for the fabrication of OPV cells and PCs; determination of the incident power density and illuminance of the indoor light sources; calculation of color coordinates on the CIE xy 1931 Chromaticity Diagram; mechanism of 1D PCs in the manipulation of the light color; calculated transmittance of the other design PC structures (Fig. S1); normalized absorptance and transmittance spectra of the neat donor and acceptor films (Fig. S2); transmittance spectra and the transmitted power intensity spectra of transparent OPV devices (PM6:O-IDTBR and PTB7-Th:ITIC) and devices combined with PCs (Fig. S3); chromaticity diagrams of PTB7-Th:ITIC- and PM6:O-IDTBR-based devices in combination with PCs (Fig. S4); CIE XYZ standard observer color matching functions (Fig. S5); emission power and the integrated power spectra of 2700 K LED light at 1000 lux (Fig. S6); atomic force microscope measurements of layer thickness and toughness (Fig. S7); spectral luminous efficiency function for human photopic vision (Fig. S8); and photonic band structure schematics (Fig. S9).

There are no conflicts to declare.

This work was supported by the National Natural Science Foundation of China (No. 11774204) and the Major Program of Natural Science Foundation of Shandong Province (No. ZR2019ZD43). X.T.H also acknowledges support from the ARC Centre of Excellence in Exciton Science (No. CE170100026). Y.H. thanks the Qilu Young Scholar Program of Shandong University (No. 11160082063115).

DATA AVAILABILITY

The data that support the findings of this study are available within the article and its supplementary material.

REFERENCES

[1]B. P. Lechêne, M. Cowell, A. Pierre, J. W. Evans, P. K. Wright, and A. C. Arias, Nano Energy **26**, 631 (2016).
[2]M. Mainville and M. Leclerc, ACS Energy Lett. **5**(4), 1186 (2020).
[3]S. Shin, C. W. Koh, P. Vincent, J. S. Goo, J. Bae, J. Lee, C. Shin, H. Kim, H. Y. Woo, and J. W. Shim, Nano Energy **58**, 466 (2019).
[4]Y. J. You, C. E. Song, Q. V. Hoang, Y. Kang, J. S. Goo, D. H. Ko, J. J. Lee, W. S. Shin, and J. W. Shim, Adv. Funct. Mater. **29**, 1901171 (2019).
[5]M. Nam, H. Y. Noh, J. Cho, Y. Park, S. C. Shin, J. A. Kim, J. Kim, H. H. Lee, J. W. Shim, and D. H. Ko, Adv. Funct. Mater. **29**(16), 1900154 (2019).
[6]Y. Cui, H. Yao, T. Zhang, L. Hong, B. Gao, K. Xian, J. Qin, and J. Hou, Adv. Mater. **31**(42), e1904512 (2019).
[7]Y. Cui, Y. Wang, J. Bergqvist, H. Yao, Y. Xu, B. Gao, C. Yang, S. Zhang, O. Inganäs, F. Gao, and J. Hou, Nat. Energy **4**(9), 768 (2019).
[8]Z. Ding, R. Zhao, Y. Yu, and J. Liu, J. Mater. Chem. A **7**(46), 26533 (2019).
[9]L. Ma, Y. Chen, P. C. Y. Chow, G. Zhang, J. Huang, C. Ma, J. Zhang, H. Yin, A. M. Hong Cheung, K. S. Wong, S. K. So, and H. Yan, Joule **4**(7), 1486 (2020).
[10]H. Yin, J. K. W. Ho, V. Piradi, S. Chen, X. Zhu, and S. K. So, Small Methods **4**, 2000136 (2020).
[11]J. K. W. Ho, H. Yin, and S. K. So, J. Mater. Chem. A **8**(4), 1717 (2020).
[12]X. Ma, J. Wang, J. Gao, Z. Hu, C. Xu, X. Zhang, and F. Zhang, Adv. Energy Mater. **10**(31), 2001404 (2020).
[13]S. Park, H. Ahn, J. Kim, J. B. Park, J. Kim, S. H. Im, and H. J. Son, ACS Energy Lett. **5**(1), 170 (2020).
[14]Y. Cho, T. Kumari, S. Jeong, S. M. Lee, M. Jeong, B. Lee, J. Oh, Y. Zhang, B. Huang, L. Chen, and C. Yang, Nano Energy **75**, 104896 (2020).
[15]E. Yablonovitch, Phys. Rev. Lett. **58**(20), 2059 (1987).
[16]S. John, Phys. Rev. Lett. **58**(23), 2486 (1987).
[17]H. Jiang, H. Chen, H. Li, Y. Zhang, J. Zi, and S. Zhu, Phys. Rev. E **69**(6), 066607 (2004).
[18]H. Jiang, H. Chen, H. Li, Y. Zhang, and S. Zhu, Appl. Phys. Lett. **83**(26), 5386 (2003).
[19]Y. Fink, J. N. Winn, S. Fan, C. Chen, J. Michel, J. D. Joannopoulos, and E. L. Thomas, Science **282**(5394), 1679 (1998).
[20]M. Mulot, M. Swillo, M. Qiu, M. Strassner, M. Hede, and S. Anand, J. Appl. Phys. **95**(10), 5928 (2004).
[21]E. Özbay and B. Temelkuran, Appl. Phys. Lett. **69**(6), 743 (1996).
[22]J. C. Knight, Nature **424**, 847 (2003).
[23]J. Zimmermanna, M. Kampa, A. Forchela, and R. Märzb, Opt. Commun. **230**, 387 (2004).
[24]J. J. Wierer, A. David, and M. M. Megens, Nat. Photonics **3**(3), 163 (2009).
[25]E. Kuramochi, J. Mater. Chem. C **4**(47), 11032 (2016).
[26]B. Liu, G. Lu, L. Cui, J. Li, F. Sun, F. Liu, Y. Li, T. Yang, and G. Du, Opt. Express **25**(12), 13271 (2017).
[27]M. Fox, *Optical Properties of Solids*, 2nd ed. (Oxford University Press, United Kingdom, 2010).
[28]H. K. H. Lee, Z. Li, J. R. Durrant, and W. C. Tsoi, Appl. Phys. Lett. **108**(25), 253301 (2016).
[29]G. A. H. Wetzelaer, M. Kuik, and P. W. M. Blom, Adv. Energy Mater. **2**(10), 1232 (2012).
[30]Y. Zhou, T. M. Khan, J. W. Shim, A. Dindar, C. FuentesHernandez, and B. Kippelen, J. Mater. Chem. A **2**(10), 3492 (2014).
[31]N. K. Elumalai and A. Uddin, Energy Environ. Sci. **9**(2), 391 (2016).

Published under license by AIP Publishing